

ON THE BONDING AND REACTIVITY OF CO₂ ON METAL SURFACES

H.-J. FREUND

*Institut für Physikalische und Theoretische Chemie der Friedrich-Alexander-Universität
Erlangen-Nürnberg, Egerlandstrasse 3, D-8520 Erlangen, Fed. Rep. of Germany
and
General Electric Research and Development, Schenectady, New York, 12301, USA*

and

R.P. MESSMER

General Electric Research and Development, Schenectady, New York 12301, USA

Received 18 November 1985; accepted for publication 24 January 1986

We present ab-initio valence-bond calculations on free and coordinated CO₂. By analogy to transition-metal complexes with coordinated CO₂ three different coordination geometries for the CO₂ molecule are considered: (a) pure carbon coordination, (b) pure oxygen coordination, (c) mixed carbon–oxygen coordination. It is shown that pure oxygen ((b) geometry) and mixed carbon–oxygen coordination ((c) geometry) are more favourable than pure carbon coordination. In all cases studied, the bonding between the CO₂ moiety and the metal atom is described best as a CO₂[−] anion interacting with a Ni cation. On the basis of the theoretical calculations, many observed and expected features (some already known and some predicted) of the interaction of CO₂ and metal surfaces can be discussed. The electron transfer to the CO₂ moiety drives the observed bent geometry of the coordinated CO₂ molecule and is accompanied by an elongation of the C–O bond distance with respect to the free molecule. The bond elongation leads to a drastic lowering of the asymmetric C–O stretching frequency, and a change in the relative energy position of the photoelectron peaks. We also consider intermolecular interaction between the CO₂[−] anion and surrounding neutral CO₂ molecules via “solvation” in analogy to results of recent gas-phase cluster experiments. On the basis of the deduced metal–CO₂ bonding scheme the reactivity of coordinated CO₂ is investigated. Three reaction channels are considered: (a) dissociation into CO and O[−], (b) oxidation to CO₃[−] and CO₃^{2−}, (c) disproportionation of CO₂[−] + CO₂ to CO₃[−] and CO. On the basis of energetic considerations we argue that dissociation is likely to occur on transition-metal surfaces, while oxidation to carbonate species is more likely on noble metals due to the low binding energies for the dissociation products, namely oxygen and CO on these surfaces.

1. Introduction

In contrast to the extensive number of experimental and theoretical studies on the adsorption of CO on metal surfaces [1–5], adsorption of CO₂ has received little attention. Only recently, have groups started to study the

adsorption of CO₂ using the spectroscopic machinery of surface science [6–23]. One reason for the growing interest in CO₂ adsorption is that it can serve as an inexpensive reagent in selected reduction processes [24]. For example, in methanation reactions employing Ni-based catalysts, CO₂ reaction proceeds more rapidly than that of CO and at lower temperatures [25]. Another reason for the interest in CO₂ reactions on surfaces is due to the formation of a Boudouart equilibrium $2\text{CO} \rightarrow \text{C} + \text{CO}_2$ [26] in connection with CO-based methanation reactions [27,28]. In order to understand CO₂ reactions from the viewpoint of surface science one wants first to gain insight into the interactions between CO₂ and transition metals, and subsequently consider possible reactions of the interacting species. As far as the reactivity of CO₂ is concerned we consider three sets of experimental observations reported in the literature to be particularly important.

(1) On transition-metal surfaces reactions have been observed which are interpreted as dissociation of CO₂ into CO and oxygen [5,8,9,12]. In this connection the results on the reverse reaction, namely the oxidation of CO to form CO₂, reported by Ertl's group, are of particular interest [3,29,30].

(2) On Ag surfaces it is claimed that CO₂ reacts with surface oxygen to form a carbonate [14–21]. The formation of carbonate species has also been postulated on transition-metal surfaces, under certain conditions [10,11].

(3) On supported metal surfaces a wide variety of adsorbed species (formed from CO₂) have been identified using IR-vibrational spectroscopies [22,23].

To the best of our knowledge, no theoretical study of a model system is available thus far to elucidate the bonding of CO₂ to transition metals. Such a study, however, might provide considerable insight into the possible reactions an adsorbed molecule may undergo. Thus, in the present paper we report results of *ab-initio* generalized valence-bond (GVB) calculations [31] of free and coordinated CO₂. As in previous work on CO and N₂ transition-metal bonding, where analogies to transition-metal complexes [32–35] were very valuable, we appeal to available information on the structure and reactivity of transition-metal complexes [36–38] containing CO₂, in order to set up a model study. CO₂ is known to exist in two bonding modes in transition-metal complexes, as schematically shown in fig. 1. In both cases (I [39] and II [40]) the CO₂ is bent, and the C–O bond lengths have increased beyond the value in the free CO₂ molecule. In case I, the bent CO₂ molecule is asymmetrically distorted and the longer C–O bond is coordinated to a single metal center [39]. The metal is located closer to the carbon than to the oxygen atom. In case II the molecule is symmetrically distorted with respect to free CO₂ and coordinated to several metal atoms through both the carbon and the oxygen atoms [40]. The lengths of the two C–O bonds in II are comparable to those in I. Although there are no data available on the thermodynamic stability of either type of compound, II seems to be much more stable than I as judged from their relative chemical stabilities. Recently, Sakaki et al. [41] reported the

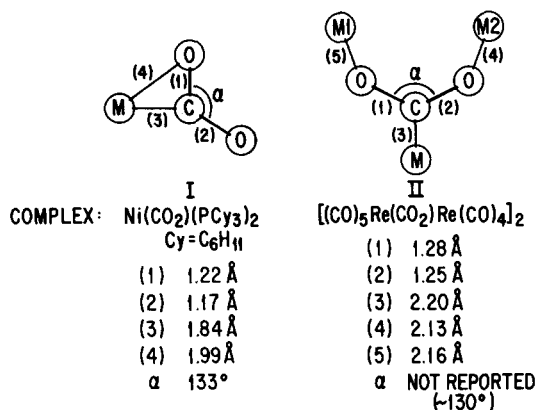


Fig. 1. Schematic representation of the bonding modes of CO₂ in transition-metal complexes. Specific structural parameters are given for two examples: Ni(CO₂)(PCy₃)₂ [39], and [(CO)₅Re(CO₂)Re(CO)₄]₂ [40].

results of an ab-initio Hartree-Fock study on (PH₃)₂NiCO₂ (type I) and calculated a bond energy of 27 kcal/mol with respect to dissociation into (PH₃)₂Ni and CO₂. They analyze their results in terms of an energy-partitioning procedure and find electrostatic as well as a π back-donation interaction between (PH₃)₂Ni and CO₂ to be the contributors to the stability of the complex. In the same paper, Sakaki et al. [41] investigated the relative stability of type I and type II coordination and find type I to be more stable than type II.

The rationale for considering these molecular complexes as models to discuss the bonding and reactivity of adsorbed CO₂ becomes apparent if we recall the structures for O + CO(2 × 1) coadsorption suggested by Conrad et al. [29] as possible intermediates in the CO oxidation:



(Langmuir-Hinshelwood mechanism [30]).

Schematically, the proposed structure of the coadsorbed CO and O species on Pd(111) [29] is shown in fig. 2a. Fig. 2b indicates the details of the adsorbate-metal and the adsorbate-adsorbate interatomic distances. The distance between the carbon atom of CO and the adjacent chemisorbed oxygen is 2.7 Å [29]. Even though this distance is well beyond the equilibrium distance in CO₂, which is 1.16 Å [42], it is in the region of the potential energy curve for CO₂ dissociation into CO(¹Σ) and O(³P), where the system exhibits some binding [43]. This is indicated in the lower panel of fig. 2b. Therefore, coordinated CO₂ species such as found in CO₂-transition-metal complexes (fig. 1) may be regarded as possible models for intermediates in CO oxidation, as well as in the reverse reaction - CO₂ dissociation.

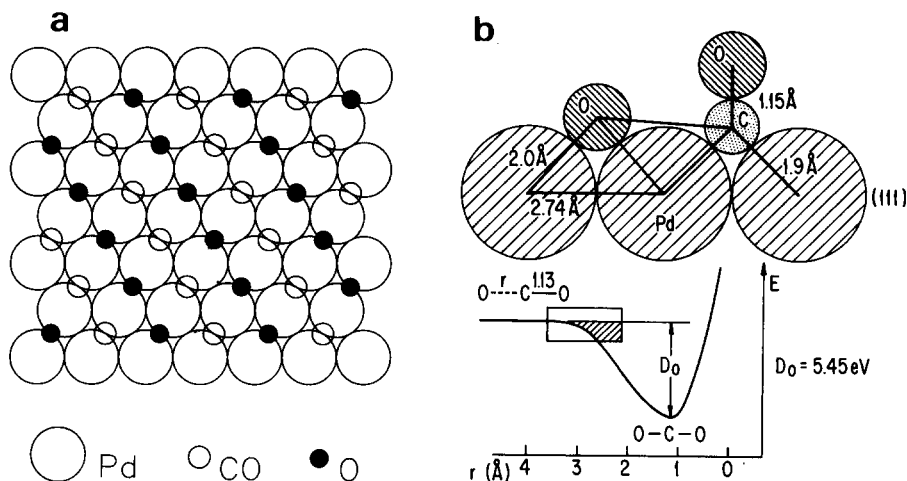


Fig. 2. Structure of the $[O + CO(2 \times 1)]/Pd(111)$ coadsorbate system as taken from Conrad et al. [29]: (a) top view; (b) side view with details of the structural parameters as derived from LEED. The potential energy curve for CO₂ dissociation into CO and O is taken from ref. [43].

A key point in the present paper is the crucial role that the anion, CO₂⁻, plays in the bonding and reactivity of CO₂. The CO₂⁻ anion is known to exist in the gas phase [44–46], and to be metastable with respect to the autodetachment process [46]:



with an activation energy of ≈ 0.4 eV [45]. The CO₂⁻ anion is bent and has C_{2v} symmetry [44,45,47–50]. Due to the negative electron affinity of CO₂ (-0.6 eV) [52], CO₂⁻ has a lifetime of only 60–90 ms [46,52]. However, as has been shown by very recent experiments on CO₂ clusters [53,54], the anion can be solvated by other neutral CO₂ molecules, to form e.g. CO₂⁻ · CO₂ dimers which actually have a positive electron affinity of 0.9 eV [55], thus leading to a stable anionic dimer moiety. Even though CO₂⁻ loses some of its anionic character after coordination to the metal atom the intermediate formation of a CO₂⁻ anion helps us to explain in a very simple fashion why CO₂ becomes bent when coordinated and also why it can be unsymmetrically distorted (with two different CO bond lengths) upon coordination. The present approach leads to a straightforward explanation of the two bonding modes of CO₂ in complexes (see fig. 1). Furthermore, knowing the electronic structure of the final dissociation products, e.g. CO and O⁻, and their bonding towards transition metals we are able to propose reaction paths for the dissociation of CO₂, and, conversely, CO oxidation. Also, based on the formation of the anion we shall propose a mechanism for the formation of carbonate species involving the anionic dimer

complex (CO₂⁻ · CO₂). Again, direct analogies can be drawn from the structure and reactivity of transition-metal complexes. From energetic considerations we find that formation of carbonate species should be preferred over CO₂ dissociation on noble-metal surfaces, while the reverse should be true in general for transition metals. Exceptions are discussed.

In section 2 we briefly discuss the theoretical methods used for the present calculations and in section 3 a discussion is given which relates the calculations to some of the issues just raised.

2. Computational aspects

The basis set for the first-row atoms (C, and O) used in the calculations were of valence double zeta plus polarization quality [56]. For the calculations of the negative ions we augmented the valence double zeta basis set with one set of Rydberg-like p function as recommended by Dunning and Hay [56]. For Ni, the Ar core was replaced by a modified effective potential [57], the 3d, 4s, and 4p basis sets were of double zeta quality [58]. The s combination of d-type basis functions were excluded.

The following systems have been calculated: CO₂ (D_{∞h}, ¹Σ⁺) in the experimentally determined equilibrium geometry (C–O: 1.16 Å); CO₂⁻ (D_{∞h}, ²Π) in the same geometry as CO₂; CO₂⁻ (C_{2v}, ²A₁) in the geometry optimized at the Hartree–Fock level [47–50] (C–O: 1.22 Å, angle C–O–C: 133°); CO₃²⁻ (D_{3h}, ¹A⁺) in the geometry experimentally found in inorganic carbonates (C–O: 1.27 Å, angle O–C–O: 120°); Ni atom (³D); Ni positive ion (²D); oxygen atom (³P); oxygen anion (²P); NiCO₂ (C_{2v}, ¹A₁) with the CO₂ moiety in the geometry of the bent CO₂⁻ anion and bond distances as given in fig. 3a; CO₂Ni (C_{2v}, ³A₁) with the CO₂ moiety as above, and bond lengths as indicated in fig. 3b; NiCO₂ (C_s, ¹A) in the geometry experimentally found for complex I [39] in fig. 1, and with shorter Ni–C (1.75 Å) and Ni–O (1.9 Å) bonds as compared to the experimentally found geometry [39] (see fig. 3c). In all calculations the GVB perfect-pairing (PP) [31] wavefunctions were obtained. For neutral CO₂ as well as linear and bent CO₂⁻, 16 valence electrons were paired into 8 correlated pairs. For NiCO₂, 13 pairs were formed: 8 pairs for the CO₂ moiety, 4 pairs for the Ni d electrons, and an additional pair formed between the remaining Ni d electron and the unpaired electron on CO₂⁻. For the CO₂Ni calculation 12 pairs were formed. Two unpaired electrons remain, one each on the Ni and the CO₂⁻, respectively. They are coupled into a triplet. For the Ni atom 4 pairs of d electrons were formed, and the remaining two s and d electrons were coupled to form a triplet. For the Ni ion the electrons were coupled to form 4 pairs, leaving one d electron unpaired. In the case of the carbonate anion 12 pairs were formed. For the oxygen atom 2 pairs were formed, and the remaining electrons were triplet coupled. In the

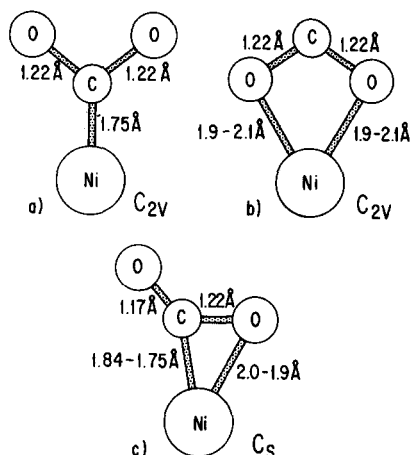


Fig. 3. Schematic representation of the three coordination modes of CO₂. Indicated structural parameters have been used in the calculations described in the text: (a) pure carbon coordination; (b) pure oxygen coordination; (c) mixed carbon-oxygen coordination.

Table 1
Calculated total energies

System	Type of calculation	Basis set ^{a)}	Energies (au)	
Ni (³ D)	GVB-PP (4 pairs)	VDZ + POL	-40.55891	
	Hartree-Fock	VDZ + POL	-40.54050	
Ni ⁺ (² D)	GVB-PP (4 pairs)	VDZ + POL	-40.26647	
	Hartree-Fock	VDZ + POL	-40.24760	
O (³ P)	GVB-PP (2 pairs)	VDZ + POL + RYD	-74.81762	
O ⁻ (² P)	GVB-PP (3 pairs)	VDZ + POL + RYD	-74.81761	
	Hartree-Fock	VDZ + POL + RYD	-74.77994	
CO ₂ (¹ Σ ⁺)	GVB-PP (8 pairs)	VDZ	-187.65064	
	GVB-PP (8 pairs)	VDZ + POL	-187.77632	
	GVB-PP (8 pairs)	VDZ + POL + RYD	-187.77632	
	Hartree-Fock	VDZ + POL + RYD	-187.67447	
	Hartree-Fock	VDZ	-187.60062	
CO ₂ ⁻ (² Π)	GVB-PP (8 pairs)	VDZ	-187.60062	
	GVB-PP (8 pairs)	VDZ + POL	-187.69316	
	GVB-PP (8 pairs)	VDZ + POL + RYD	-187.71936	
	Hartree-Fock	VDZ + POL + RYD	-187.62726	
	Hartree-Fock	VDZ	-187.62726	
CO ₃ ²⁻ (¹ A)	GVB-PP (12 pairs)	VDZ + POL + RYD	-262.52903	
	GVB-PP (12 pairs)	VDZ + POL + RYD	-262.37114	
NiCO ₂ (¹ A ₁)	GVB-PP (13 pairs)	VDZ + POL + RYD	-228.27206	
	Hartree-Fock	VDZ + POL + RYD	-228.08377	
NiCO ₂ (¹ A)	C-1.85-Ni-2.0-O	GVB-PP (13 pairs)	VDZ + POL + RYD	-228.30832
	C-1.75-Ni-1.9-O	GVB-PP (13 pairs)	VDZ + POL	-228.31506
	C-1.75-Ni-1.9-O	GVB-PP (13 pairs)	VDZ + POL + RYD	-228.31795
	C-1.75-Ni-1.9-O	Hartree-Fock	VDZ + POL + RYD	-228.12941
	C-1.75-Ni-1.9-O	Hartree-Fock	VDZ	-228.12941
CO ₂ Ni (³ A ₁)	Ni-2.1-O	GVB-PP (12 pairs)	VDZ + POL + RYD	-228.31679
	Ni-1.9-O	GVB-PP (12 pairs)	VDZ + POL + RYD	-228.32514
	Ni-1.9-O	Hartree-Fock	VDZ + POL + RYD	-228.21388

^{a)} VDZ: valence double zeta, POL: polarization functions, RYD: Rydberg functions.

Table 2
Electron affinities, ionization potentials, and dissociation energies

System	Type of calculation	EA (eV)	IP (eV)	Dissociation energies into	
				Ions	Neutrals
Ni	GVB		7.96 (7.633) ^{a)} [62]		
O	GVB	0.0 (1.46) ^{a)} [72]			
CO ₂	GVB1 ^{b)}	-1.361			
	GVB2 ^{c)}	-2.263			
	GVB3 ^{d)}	-1.136 (-0.6) ^{a)} [52]			
CO ₃ ²⁻ (D _{3h})	HF	-1.285			
	GVB			-0.22	
NiCO ₂ (C _{2v})	HF			-0.98	
	GVB			7.79	-1.72 (<u>-0.86</u>) ^{e)}
CO ₂ Ni (C _{2v})	HF			5.68	-3.57
	GVB			9.01	-0.50
Ni-1.9-O	GVB			9.23	-0.28 (<u>+0.58</u>) ^{e)}
	HF			9.2	-0.03
NiCO ₂ (C _s)	GVB			9.04	-0.47 (<u>+0.39</u>) ^{e)}
	HF			6.93	-2.33

^{a)} Experimental result taken from the reference indicated.

^{b)} GVB-PP calculation using VDZ basis set.

^{c)} GVB-PP calculation using VDZ + POL basis set.

^{d)} GVB-PP calculation using VDZ + POL + RYD basis set.

^{e)} Underlined numbers are dissociation energies after inclusion of correction.

case of the oxygen anion 3 pairs have been formed, leaving one electron unpaired. The total energies of the GVB-PP calculations are given in table 1. In addition to the GVB-PP results, total energies obtained from Hartree-Fock calculations employing the same basis sets as for the GVB calculations are given for comparison. Electron affinities, ionization potentials, and binding energies obtained as total energy differences from the values in table 1 are collected in table 2. If the corresponding quantities are known experimentally they are included in table 2 for comparison. In figs. 4-6 the GVB orbital contour plots are shown. These plots will serve as the basis for the later discussion of the bonding between CO₂ and a metal atom. Fig. 4 shows the orbitals for the CO₂ molecule, and fig. 5 shows the orbital plots for bent CO₂⁻. Fig. 6 shows the relevant orbitals of the various NiCO₂ clusters to illustrate the interaction between the CO₂ moiety and the Ni atom. Fig. 7 summarizes schematically the various wavefunctions obtained, including those of the carbonate anion.

3. Results and discussion

3.1. Understanding the Ni–CO₂ bond

We choose to think of the Ni–CO₂ bond formation by considering the following Born–Haber cycle; first, ionize the Ni atom, then transfer the detached electron onto a CO₂ molecule, and thirdly bind the CO₂[−] anion to the Ni cation. As pointed out in the course of the ensuing discussion, this Gedankenexperiment enables one to visualize the various possible interactions taking place between Ni atom and the CO₂ molecule.

Fig. 4 shows the one-electron orbitals of neutral CO₂ in the ground state as obtained from a GVB-PP calculation which imposes no symmetry restrictions on the orbitals of the wavefunction. In other words we do not force the

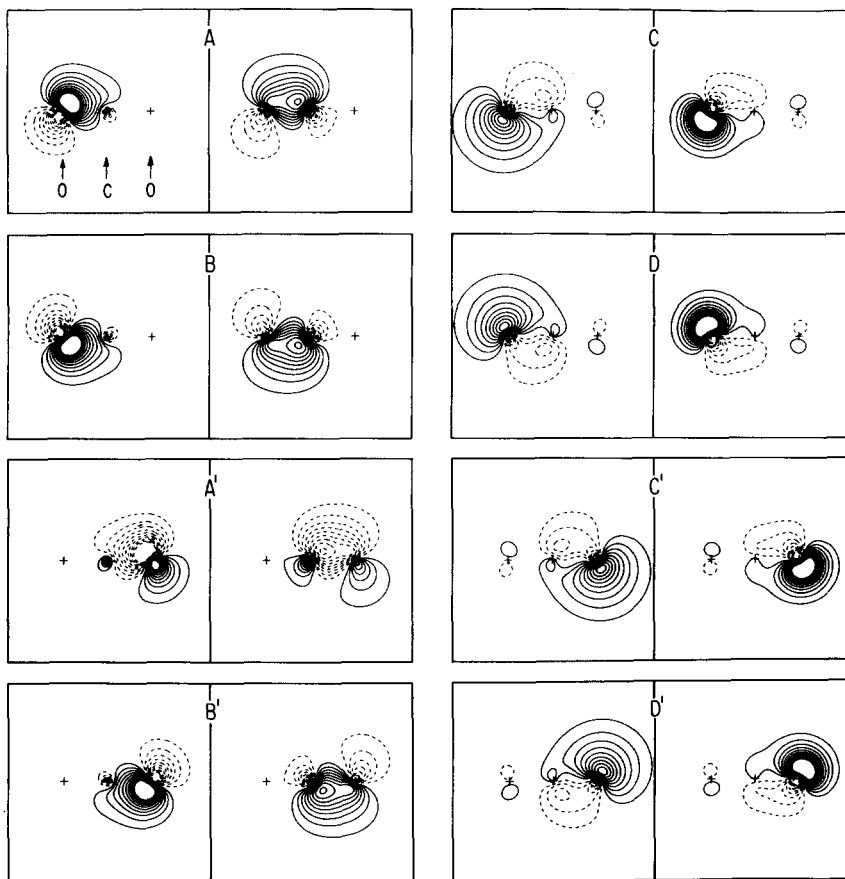


Fig. 4. One-electron orbital contour plots of the GVB pairs of linear CO₂ (see text section 3.1)

one-electron orbitals to transform according to σ or π symmetry. Only the symmetry of the total wavefunction – and not that of the orbitals – has to transform according to σ , π , δ , ..., symmetry. If a particular valence-bond structure does not have the proper overall symmetry, this symmetry is restored by “resonating” the two equivalent component GVB-PP wavefunctions (indicated for example in fig. 7a) using the so called R-GVB approach [59]. The result for the one-electron orbitals is intuitively very appealing. The carbon in the center of the molecule forms four equivalent bonds to the oxygen atoms, namely two sets of double bonds which are pairwise in planes perpendicular to each other as shown in panels A, B and A', B' of fig. 4. The electrons in the C–O bonds are left–right correlated and polarized towards the oxygen atoms as expected on the basis of the higher electronegativity of oxygen as compared to carbon. This is also seen in the charge distribution as revealed by a Mulliken population analysis; O: 8.33 e , C: 5.35 e . The remaining oxygen electrons form lone pairs in the plane perpendicular to the plane of the adjacent carbon–oxygen double bonds (panels C, D and C', D' of fig. 4). Therefore, both carbon and oxygen appear to be sp^3 hybridized and form their bonds by overlapping the sp^3 hybrid functions. This is shown schematically in fig. 7a. Clearly, the two components of the double bond can no longer be termed σ and π , as this usual symmetry along the intermolecular axis does not exist now. Moreover, this description yields a total energy for CO₂ which is lower than the corresponding values calculated by imposing the normal orbital symmetry restrictions. Until very recently [61], it has not proven possible to generate bent bonds (Ω bonds) that are energetically more stable than a σ – π description on the basis of an ab-initio approach, although the conceptual advantage of such a description was pointed out by Pauling and others over 25 years ago [60]. A thorough discussion of this description with appropriate reference to the history of the problem is presented elsewhere [61]. As shown in fig. 7a there are two resonance structures contributing to the total wavefunction. To properly calculate the resonance stabilization eight electron pairs have to be taken into account. However, the main part of the stabilization results from resonating the Ω bonds. This reduces the numerical problem considerably since it involves only four pairs. On the basis of this calculation we find a resonance stabilization of 0.7 eV.

The utility of this description for CO₂ becomes obvious when we add an electron to the molecule. The orbitals of the CO₂⁻ ion in its bent form are shown in fig. 5. Both C–O bonds are elongated by 0.06 Å with respect to neutral CO₂, and the bond angle is 133°. Clearly, the one-electron orbitals and the total wavefunction do not transform according to the symmetry of the molecule (C_{2v}), but the latter can be restored by resonating the two GVB-PP wavefunctions indicated in fig. 7b. The one-electron orbitals (perfect-pairing (PP) orbitals) in fig. 5 indicate how the molecule is able to accommodate the extra electron: it has to break one bond of a set of double bonds, forming a

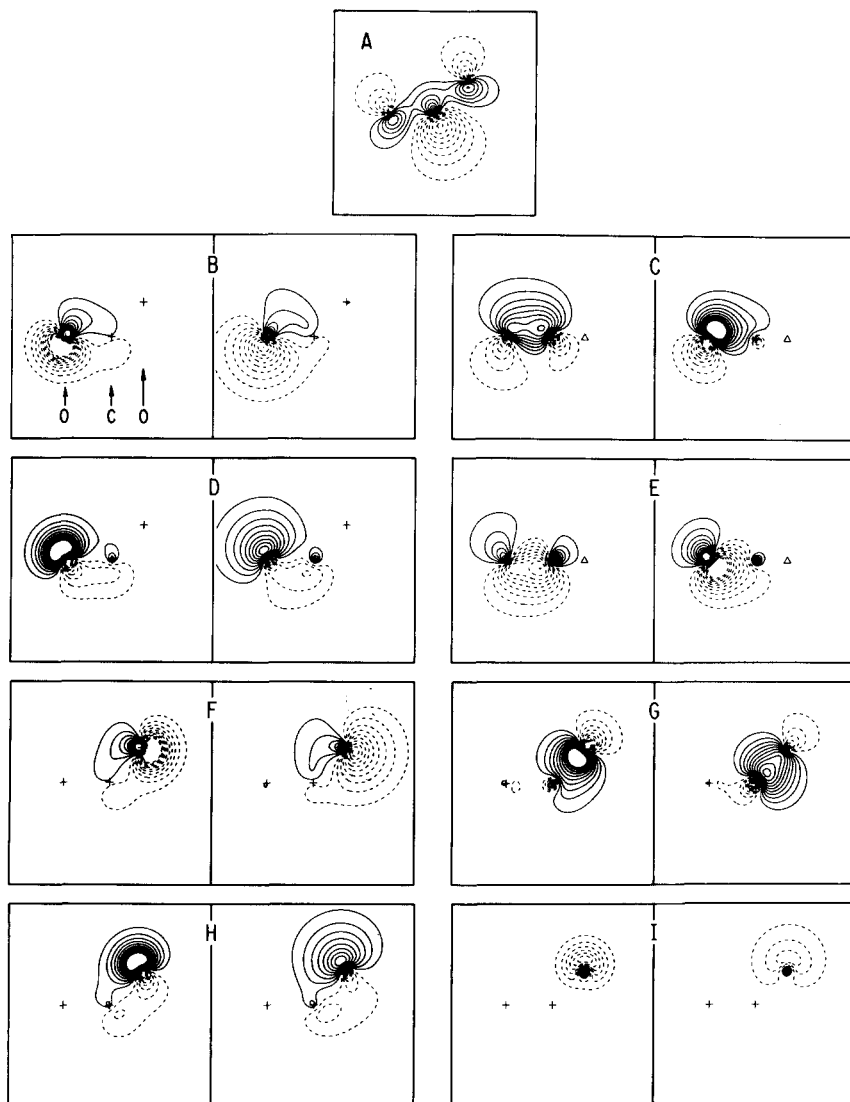


Fig. 5. One-electron orbital contour plots of the GVB pairs and the unpaired electron (panel A) of bent CO₂⁻ (see text section 3.1).

third oxygen lone pair and a single C–O bond, leaving the extra electron in the carbon dangling bond. This process only involves one half of the molecule leaving the other half as in the neutral molecule. This is clear from a comparison of panels B, C, D, and E in fig. 5 with the corresponding ones in fig. 4. The single bond and the three lone pairs are shown in panels F through

of fig. 5. The single electron shown in panel A has its largest amplitude on the carbon atom. According to fig. 5 all atoms want to keep their sp^3 hybridization upon electron attachment, and as a natural consequence the stable geometry of the CO_2^- anion has to be bent. A schematic representation of the electronic structure of the anion is shown in fig. 7b. The total electron distribution taken from a Mulliken population analysis is O: 8.62 e , and C: 5.83 e . Again, as in CO_2 , there are two resonance structures which are important (see fig. 7b). We estimate the resonance stabilization to be similar (to within a few tenth of an eV) to that calculated for CO_2 . Therefore in the following we calculate total energy differences ignoring possible differences in resonance energies.

Based on the total energies in table 1 we calculate an electron affinity of -1.14 eV for the bent CO_2^- anion as compared to the experimental value of -0.6 eV [52]. It is well known from several theoretical studies on CO_2^- [47–51] that an accurate prediction of the electron affinity can only be achieved by including extensive configuration interaction [50] to account for the different electron-correlation effects between the neutral molecule and the anion. The results of our calculations support this conclusion as indicated by a comparison of calculated electron affinities presented in table 2. GVB-PP calculations employing basis sets of increasing flexibility show that a valence double zeta (VDZ) basis set already yields an electron affinity (-1.36 eV) only slightly inferior to the result of a full VDZ plus polarization (POL) plus Rydberg functions (RYD) (see section 2) calculation (-1.14 eV). Disregarding the Rydberg functions leads to a very poor description of the electron affinity (-2.26 eV). This is entirely due to the poorer description of the anion as compared to the neutral, since the total energy of the neutral, linear molecule is only very slightly affected by inclusion of Rydberg functions after addition of polarization functions (see table 1). (Note, that a Hartree–Fock calculation using the full basis set yields a value of -1.29 eV for the electron affinity. A similar strong dependence on basis sets in the calculation of the CO_2 electron affinity using the Hartree–Fock approximation has been discussed by England [49].) Consequently, this introduces an error of ≈ 0.54 eV in the total energy of the anion with respect to the neutral. This error will be propagated when we compare the total energy of the $NiCO_2$ system (in which CO_2 assumes properties similar to CO_2^-) with that of the separated system of a Ni atom and a neutral CO_2 molecule.

In the following we investigate the bonding between CO_2 and a Ni atom. Three different sets of calculations have been carried out according to the three types of CO_2 coordination shown in fig. 3. The choice of these coordination configurations was mainly dictated by the structures found experimentally in CO_2 transition-metal complexes [36–38] as indicated in fig. 1 and discussed in section 1. The configurations chosen cover the main possible types of CO_2 –metal interaction, namely: (a) pure carbon–metal coordination (fig. 3a); (b) pure oxygen–metal coordination (fig. 3b); and (c) mixed carbon–

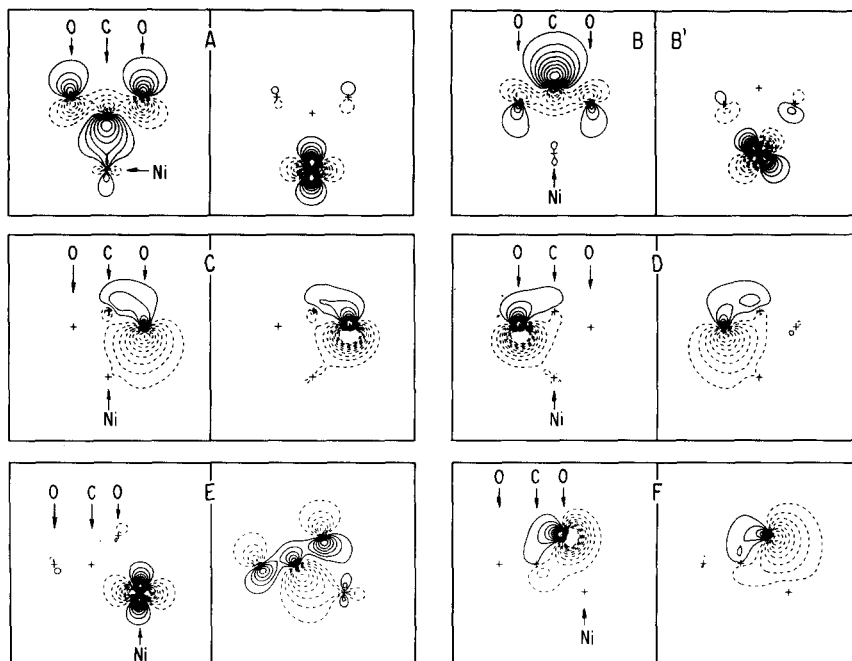


Fig. 6. One-electron orbital contour plots of selected GVB pairs and unpaired electrons in Ni-CO₂ clusters of varying geometry; Panel A: Ni-CO₂ (C_{2v}), pure carbon coordination; Panels B, C, and D: CO₂=Ni (C_{2v}), pure oxygen coordination; Panels E, and F: Ni-CO₂ (C_s) mixed carbon-oxygen coordination (see text sections 3.1.1, 3.1.2, 3.1.3).

oxygen-metal coordination (fig. 3c). The geometry of the CO₂ moiety is kept constant for all calculations, and only the relative position with respect to the Ni atom has been varied. Interestingly, the geometry of metastable CO₂⁻ is a good approximation to that found from the available structural data for coordinated CO₂ [36-38].

Before we discuss the bonding for the individual coordination configurations (a)-(c) on the basis of the PP orbitals it is necessary to comment on a general result which holds independently of the variation in geometry: All orbitals localized on the CO₂ moiety in the NiCO₂ complex have the same shapes as the orbitals of CO₂⁻ shown in fig. 5 with appropriate modifications on those interacting with the Ni atom. The Ni orbitals exhibit almost exclusively d character, indicating that the Ni fragment is basically in the d⁹ configuration of the positive ion. This general result shows, that *it is appropriate to try to understand the bonding in Ni-CO₂ by starting from CO₂⁻ and Ni⁺*. In fig. 6 we only show those orbitals of the NiCO₂ cluster that exhibit some deviation from the orbitals of the two fragments, and are needed to describe the bonding between CO₂ and Ni.

3.1.1. Pure carbon coordination (geometry of fig. 3a)

Assuming that the Ni-CO₂ system can be described as a CO₂⁻ interacting with a Ni cation, it is obvious what happens upon pure carbon coordination. In the geometry of fig. 3a the single electron on the CO₂ anion forms a bond with the single electron on the Ni atom in its d⁹ configuration. The GVB pair

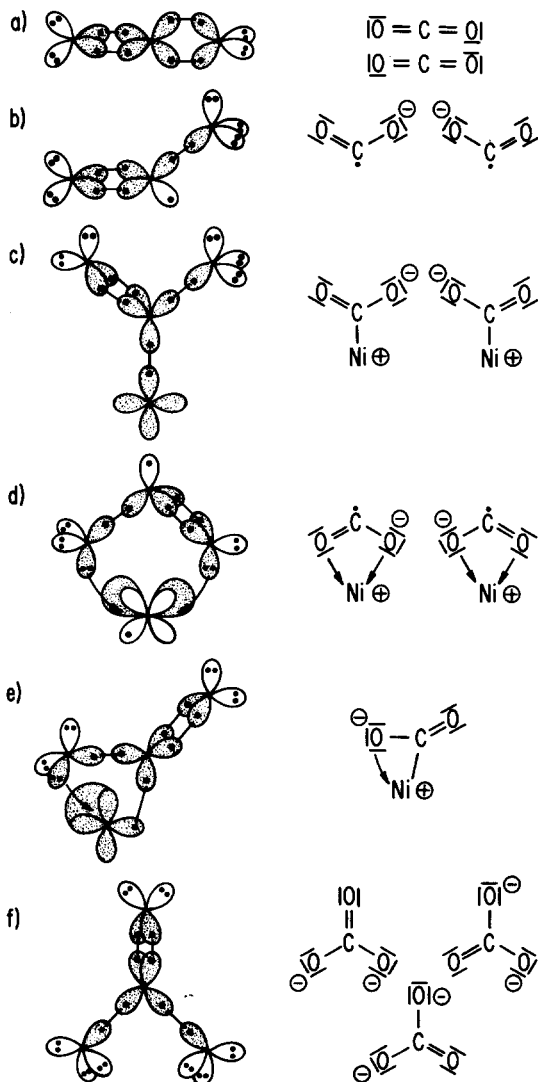


Fig. 7. Schematic representation of the many-electron wavefunctions of various systems calculated in this paper. On the right-hand side of each wavefunction representations of the corresponding valence-bond structures are shown.

representing this bond is shown in fig. 6, panel A. It is a left–right correlated pair of electrons, with one orbital of the pair localized on the CO₂[−] and the other orbital localized on the Ni atom. This CO₂ orbital looks very similar in shape to the single-electron orbital of CO₂[−] as shown in fig. 5. The Mulliken analysis gives the following atomic electron populations; C: 5.59 *e*, O: 8.47 *e*, and Ni: 9.48 *e*. Even though the results of a Mulliken population analysis can only be regarded as qualitative guidelines for the actual charge distribution, the electron transfer from the Ni atom to the CO₂ moiety (0.52 *e*) is obvious from the present result, and thus supports the approach (Ni⁺ + CO₂[−]) taken above. Fig. 7c shows a schematic representation of the many-electron wavefunction just discussed. The stabilization of the NiCO₂ system in the (a) geometry (fig. 3a) with respect to the infinitely separated parts is 7.79 eV (table 2). Obviously, the stabilization is due to the formation of the covalent bond and a Coulombic stabilization. An upper limit to the latter contribution can be estimated from Mulliken atomic charges of the separated systems to be 5.65 eV, which is 73% of the stabilization energy. Note that the corresponding total stabilization energy using Hartree–Fock energies is only 5.68 eV, which is close to the pure Coulomb stabilization energy. However, the proper reference for the total energy of the NiCO₂ system is not Ni⁺ + CO₂[−] but rather Ni + CO₂. With respect to this reference point the system is unbound by 1.72 eV (table 2). At the Hartree–Fock level it is unbound by 3.57 eV. As indicated above, this comparison using our calculated total energies is in error because the calculated affinity of CO₂ is in error by −0.54 eV (Hartree–Fock (HF): −0.69 eV). Also, as revealed by table 2 the calculated ionization potential of the Ni atom is 0.32 eV (HF: 0.34 eV) larger than experiment [62]. To correct for both errors we have to add 0.86 eV (HF: 1.02 eV) to the calculated stabilization energy. However, even including this correction leaves the NiCO₂ system in the (a) geometry unbound by 0.86 eV (HF: 2.55 eV) with respect to Ni + CO₂. Clearly, there are two resonance structures which should be taken into account for a proper description of the ground state in this geometry. However, the resonance stabilization will mainly arise on the CO₂[−] moiety, and therefore be similar to the resonance stabilization in uncoordinated CO₂[−]. Thus we expect only little influence of the resonance stabilization on the calculation of the Ni–CO₂ bond energy in this geometry. Therefore, we conclude, that the pure carbon coordination is unfavourable for CO₂ coordination.

3.1.2. Pure oxygen coordination (geometry of fig. 3b)

If we place the Ni atom on the opposite side of the CO₂ moiety as that in case (a), we achieve a geometry in which the Ni atom has a pure oxygen coordination. The geometry is shown in fig. 3b. We have chosen the Ni–O distance to be consistent with the bond lengths found in the complexes exemplified in fig. 1 [39,40]. Calculations were performed at two Ni–O distances, namely 2.1 and 1.9 Å. Both geometries lead to similar results, with

the shorter Ni–O bond leading to a slightly lower total energy (see tables 1 and 2). Therefore, we discuss the Ni–CO₂ bonding based on the latter calculation. Panels B, C and D of fig. 6 show the relevant orbitals. The system has two unpaired electrons coupled to form a triplet state. One electron resides on the Ni atom (fig. 6 panel B), the other one on the CO₂⁻ moiety pointing away from the Ni atom (fig. 6 panel B'). It has the same shape as the orbital of the unpaired electron in free CO₂⁻ (compare fig. 5 and fig. 6 panel B'). All other orbitals localized on the CO₂ moiety are identical in shape to the corresponding ones in CO₂⁻ (fig. 5) with the exception of the two oxygen lone pairs shown in panels C and D of fig. 6. Those two lone pairs establish two coordinative bonds to the Ni atom by donating their electrons into the diffuse, unoccupied s and p orbitals of the Ni atom. Due to the choice of the contours in the plotted orbitals (increment of 0.05 au) the bonding interaction between the oxygen lone pairs and the diffuse Ni orbitals shows up as an indentation in the contours of the in–out correlated lone pairs which is not present in the isolated system (fig. 5). A schematic representation of the wavefunction is given in fig. 7d. The Mulliken population analysis indicates a charge distribution similar to that of the carbon-coordinated case (fig. 3a), namely C: 5.52, O: 8.51, and Ni: 9.46 electrons. The charge transfer between CO₂ and Ni amounts to 0.54 *e* which is again comparable to case (a). However, the stability of the system has drastically improved over geometry (a). With respect to the separated ions, namely Ni⁺ and CO₂⁻, we calculate a stabilization of 9.23 eV. With respect to the separated neutrals the system is unbound by only 0.28 eV based on our total energies. This results in a state bound by 0.58 eV, once the corrections for the electron affinity of CO₂ and the ionization potential of Ni (0.86 eV, see discussion above) are taken into account.

For the present geometry the Hartree–Fock calculation yields a stabilization energy with respect to the separated parts identical to the GVB-PP calculation, namely 9.23 eV. Also, taking the appropriate corrections into account, the system is stable with respect to dissociation into CO₂ and Ni. The stabilization energy is 0.66 eV, which is even slightly better than the GVB result. Electron correlation does not seem to be crucial in this case, perhaps because the amount of covalent bonding in this case is smallest for the three geometries considered. Using the same procedure as for the (a) geometry in order to estimate the Coulombic contribution to the bonding for the present geometry one obtains 8.19 eV. This amounts to 89% of the total stabilization energy, which is considerably larger than found for the (a) geometry. The extra Coulombic stabilization the system experiences in this (b) geometry as compared to the pure carbon coordination is sufficient to account for the higher stability of the oxygen coordination. In fact, our calculations indicate that the pure oxygen coordination constitutes a favourable coordination geometry for Ni–CO₂ interaction. For the same reasons the bond energy in the (a) geometry did not depend on the resonance stabilization, the bond energy in the present

geometry does not depend on it. It should be mentioned that Jordan [63] has predicted an analogous structure for LiCO₂ on the basis of Hartree-Fock calculations. The structure of the Li salts has recently been investigated using vibrational spectroscopy [64] and the results seem to be consistent with Jordan's predictions [63].

3.1.3. Mixed carbon-oxygen coordination (geometry of fig. 3c)

The final coordination geometry considered here (the (c) geometry) is a mixed carbon-oxygen coordination (fig. 3c), which is modeled by the structure of the complex I in fig. 1. We have chosen the geometry such that the carbon-Ni and oxygen-Ni bonds are consistent with cases (a) and (b). A variation of the metal-carbon and metal-oxygen bond lengths between 1.84 and 1.75 Å, and 2.0 and 1.9 Å, respectively, showed that our GVB-PP calculations favour a smaller distance than that experimentally determined in complex I. Therefore, the following discussion is based on the results for the cluster with the shorter bond lengths. Fig. 6 shows the relevant orbitals involved in the bonding within the cluster. In view of the discussion above, it is almost unnecessary to note that all other orbitals are basically identical to the non-interacting fragments systems Ni⁺ and CO₂⁻. Panel E of fig. 6 shows the GVB pair comprising the carbon-Ni bond. Except for the asymmetry induced by the chosen geometry of the cluster the bond is very similar to the one shown in panel A of fig. 6, formed for the case of pure carbon coordination. Panel F shows the oxygen lone-pair donation into the diffuse s/p orbitals of Ni as indicated by the indentation of the lone-pair contours. Clearly, this unsymmetric coordination involves both bonding modes (a) and (b). A schematic view of the many-electron wavefunction is shown in fig. 7e. The stability of this coordination mode is almost as high as the pure oxygen coordination ((b) geometry). The stabilization energy with respect to the separated ions is 9.04 eV, and thus only 0.2 eV smaller than that for the pure oxygen coordination. The Coulomb contribution to the stabilization is only 6.47 eV (72%) which is considerably smaller than in the case of pure oxygen coordination. Since the total stabilization is similar in both cases one might argue that the amount of covalency in the bonds is larger for the unsymmetric mixed carbon-oxygen coordination.

The Mulliken population analysis supports this conclusion by indicating a smaller charge transfer (0.39 *e*) between the Ni atom and the CO₂ molecule (C: 5.57 *e*, O(coord): 8.37 *e*, O (non-coord): 8.45 *e*, and Ni: 9.61 *e*). With respect to the separated neutral fragments the present cluster is unbound by 0.47 eV. However, after the corrections (discussed above) are taken into account, the system is bound by 0.39 eV. This has to be compared with a bond energy of 0.58 eV for pure oxygen coordination. The difference of only 0.19 eV may be slightly underestimated, since in the present geometry (C_s) the resonance stabilization should be smaller than in the two geometries of the

Ni-CO₂ cluster with higher symmetry (C_{2v}). It is simply this loss of resonance stabilization compared with the symmetric geometries that is responsible for the shortening of the uncoordinated C-O bond. For the purpose of the qualitative arguments in the present paper we neglect this additional effect on the total energy differences. Similar to the situation in case (a) the (c) geometry is unbound on the basis of Hartree-Fock calculations even after accounting for the appropriate corrections. It is therefore surprising that the Hartree-Fock calculations for the (PH₃)₂NiCO₂ complex carried out recently by Sakaki et al. [41] using a comparable geometry yield a (PH₃)₂Ni-CO₂ binding energy of 1.15 eV. Our calculations suggest that one has to take account of the intra-pair correlation energy to gain a stable system. However, the relative stability of pure carbon versus mixed carbon-oxygen coordination found in this study is consistent with their results [41].

In summary, our results indicate that among the three coordination modes considered here the CO₂ molecule prefers to adopt either a mixed carbon-oxygen coordination ((c) geometry) or a pure oxygen coordination ((b) geometry) to the metal center, while a pure carbon coordination ((a) geometry) appears to be unfavourable. The approximate binding energies are 9 and 14 kcal/mol, respectively, and suggest a rather weak CO₂-transition-metal bond in agreement with the low stability of CO₂ complexes and adsorbates [3,11,12,37,65]. It seems that in the pure oxygen coordination mode the system has a large Coulomb (ionic) contribution to the CO₂ metal bond while in the mixed carbon-oxygen coordination mode the degree of covalency increases. In the following sections we will discuss intermolecular interactions in CO₂ adsorbate overlayers, the reactivity of CO₂ in complexes and adsorbates, and, finally, the spectroscopy of CO₂-transition-metal complexes and adsorbates.

3.2. Intermolecular interaction in adsorbate overlayers

Due to the rather small molecule-metal binding energies suggested from the results in section 3.1, intermolecular interactions between adsorbed molecules may be important in understanding the formation of adsorption overlayers of CO₂ on transition-metal surfaces. In order to get some idea about the intermolecular interactions between CO₂ molecules it is illustrative to recall the structure of solid CO₂ at low pressure. Fig. 8a shows a top view of the (100) plane of solid CO₂ [42]. Fig. 8c isolates a CO₂ dimer from the periodic structure to illustrate the details of the intermolecular arrangement. The T-shaped "dimer" cut out of the solid is almost degenerate energetically with the dimer formed by two parallel CO₂ molecules [66,67]. The T-shaped structure is favored by the attractive quadrupole intermolecular interactions upon formation of the solid [68]. In very recent experimental studies on CO₂ clusters [53-55] in the gas phase it was found that there exist stable anionic CO₂ clusters, the smallest of which is the CO₂⁻ · CO₂ dimer. Hershbach and

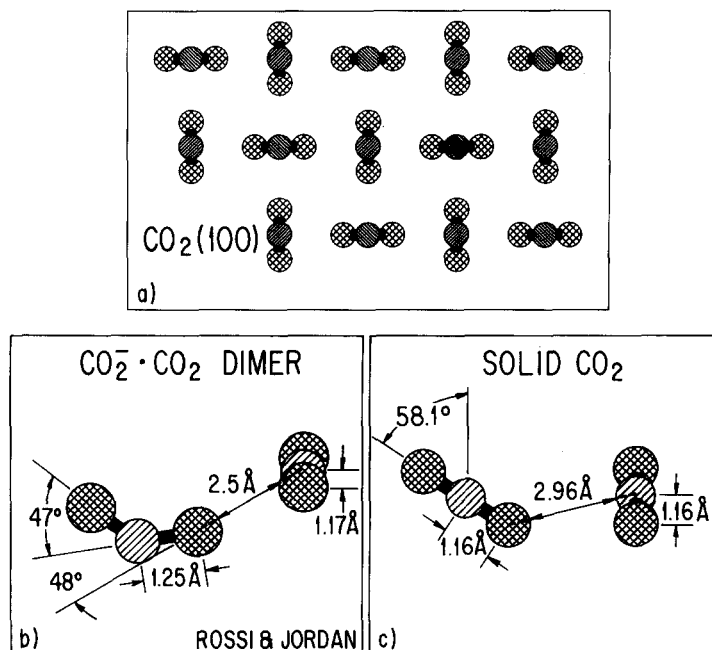


Fig. 8. (a) Top view of the (001) surface of solid CO₂ [43]. (b) Structure of the CO₂ dimer anion as calculated by Rossi and Jordan [66]. The neutral CO₂ molecule has been rotated around the "long" intermolecular C–O connection. (c) CO₂ dimer as "cut" out of the (001) surface of solid CO₂.

coworkers [55] report this cluster to have a positive electron affinity of 0.9 eV. The structure of this dimer was predicted by Rossi and Jordan [66] on the basis of geometry-optimized Hartree–Fock calculations and is shown in fig. 8b. It can be understood as a CO₂[−] anion with interatomic distances and bond angle close to the isolated anion solvated by a very slightly bent (O–C–O angle: 179°) neutral CO₂. The smallest distance between the two CO₂ moieties is 2.5 Å [66]. In order to draw the picture in fig. 8b we have rotated the quasi-linear CO₂ molecule about this long C–O "bond". In this conformation the similarity to the structure cut out of the solid is apparent. Therefore, it is plausible to assume that, at least at high local CO₂ coverages, the CO₂[−] anions are stabilized through solvation by other neutral CO₂ molecules. There is further experimental evidence for such a structure from vibrational spectroscopic studies on the matrix-isolated Li salt of the dimer anion recently reported by Kafafi et al. [64]. The differences in the local molecule–metal bond energies between pure oxygen and mixed carbon–oxygen coordination may be overcome by the stability of the dimer anion being formed. Then the question of how to pack the dimer anions on the surface becomes the important issue. As

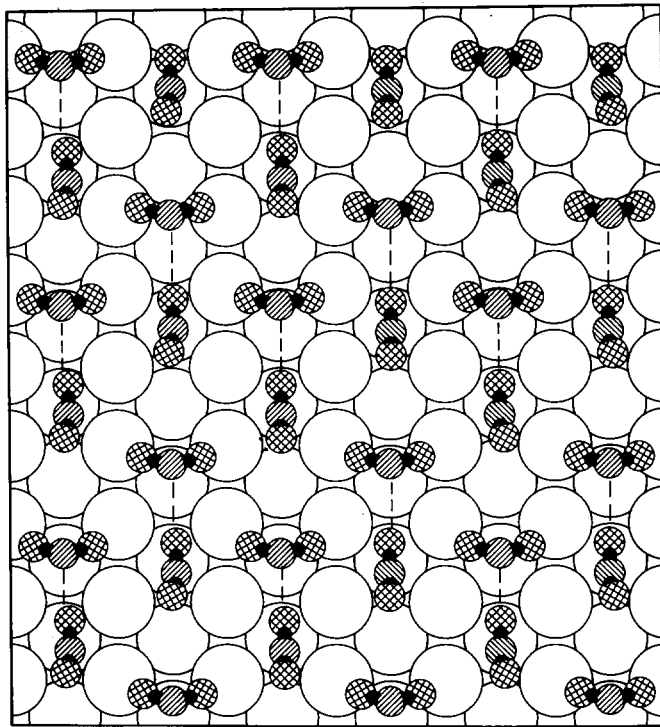


Fig. 9. Possible arrangement of the CO₂ dimer anions on a Ni(110) surface. The local binding site of the CO₂⁻ is the mixed carbon–oxygen coordination. This figure was generated with the use of D. Vanderbilt's graphics program. The atomic radii do not reflect Van der Waals radii.

an example, one possibility is shown in fig. 9, where the CO₂⁻ anions sit in the troughs of a Ni(110) surface in a local site favoring the mixed carbon–oxygen coordination and the solvating CO₂ molecules sit further above the surface bridging the troughs. Of course, *there are many other possibilities even on the same surface*. The formation of the dimer does not favor one of the two stable metal–molecule bonding modes over the other one. However, the solvation of CO₂⁻ stabilizes the anionic system by such an amount that the proposed mechanism of bonding CO₂ to the metal via formation of CO₂⁻ becomes very plausible even in the case of noble metals. In fact, the stabilization of the anionic system should, according to Hershbach and coworkers [55], be of the order of 0.9 eV, thus stabilizing even the pure carbon-coordinated system, which is unstable by 0.86 eV (see table 2) without intermolecular interaction. There is only one pure carbon-coordinated CO₂ complex known [70], and it is argued [70] that its stability is induced by inter- and intra-molecular ligand interactions within the complex.

In the solvation model discussed above the structure of the solvated anion is

chosen to simulate as closely as possible the next-neighbor structure in the CO₂(001) surface, thus favoring a T-shaped dimer. However, if one releases this restriction, and chooses a dimer with parallel orientation of CO₂ molecules [66,67], intermolecular interactions involving carbon–carbon interactions are also possible, favoring another class of reactions involving carbon–carbon bond formation.

3.3. Reactivity of transition-metal CO₂ complexes and CO₂ adsorbates

As mentioned in section 1, the reactivity of CO₂-coordinated transition-metal systems has gained some attention recently due to the possibility of activating an otherwise rather inert molecule like CO₂, which is available in large quantities as an inexpensive reagent [24]. The reactivity of CO₂ transition-metal complexes is an active field of research in organometallic chemistry, and several reviews have appeared recently [36–38]. It is interesting to refer to the experience accumulated in organometallic chemistry in order to investigate the possible reaction channels for CO₂ adsorbed on surfaces. Specifically, we want to consider three possible reaction channels: (a) dissociation of CO₂⁻ into CO and O⁻; (b) direct oxidation of CO₂⁻ by O or O⁻ to CO₃⁻ or CO₃²⁻; (c) disproportionation of solvated CO₂⁻ into CO₃⁻ and CO. Using the results of the previous sections we will discuss the three reaction channels separately.

3.3.1. Dissociation of CO₂

Fig. 10 shows the energetics (total energy differences), partly available from experiment, for the process:

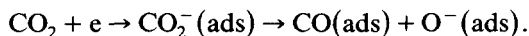


Fig. 10 has two branches: The left branch shows the energetics for the dissociation on a nickel surface while the right-hand branch shows the energetics if single Ni atoms were involved in the process. In the middle of fig. 10 infinitely separated metal (surface or two atoms) and neutral CO₂ defines the energy zero of the diagram. For reference purposes the energy necessary to rupture one C–O bond in CO₂ (5.45 eV) [43] is given. As was alluded to in section 3.1 we consider a Born–Haber cycle to outline the energetics. First, to ionize the metal it costs ≈ 2.4 eV more energy for the isolated atom [62] than for the surface [71] (7.63–5.2 eV), next to transfer the metal electron onto the CO₂ molecule costs 0.6 eV [52]. In the next step, dissociation of the CO₂⁻ anion into CO and O⁻, costs 3.4 eV (being the difference between the dissociation energy for a C–O bond in CO₂ (5.45 eV) and the sum of electron affinities of oxygen (1.46 eV) [72] and CO₂ (0.6 eV) [52]). Obviously, it is easier to dissociate an O⁻ from a CO₂ anion than a neutral oxygen from a linear CO₂ molecule. This can be easily understood by comparing the bonding in CO₂ and CO₂⁻. CO₂ has two sets of double bonds while CO₂⁻ has one set of double

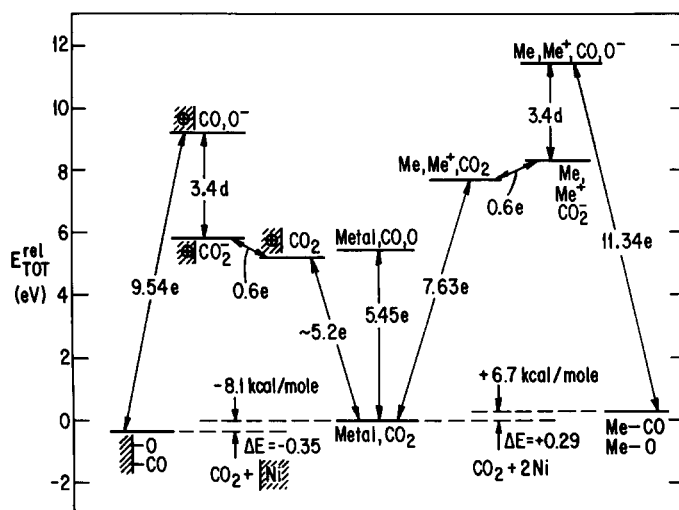


Fig. 10 Schematic total energy level diagram for the dissociation of CO₂ coordinated to a metal (surface and isolated metal atom). The energy zero (in the middle of the figure) is given by the sum of the total energies of the non-interacting constituents metal (Me) and CO₂. To the left, energies for the dissociation process on a surface have been used. On the right energies for the same process involving isolated metal atoms have been used. References are given in the text. Energies are given in eV. The letter "e" indicates that the value is taken directly from experiment, while the letter "d" indicates that the value has been derived from experimental numbers. The detached electron has been omitted.

bonds and a single bond thus decreasing the average C–O bond strength. Finally we bind the separated systems to the metal. The given energies are calculated by taking the electron from the oxygen, transferring it back to the metal and then adding the binding energies for oxygen–metal and CO–metal bond as determined experimentally for single metal atoms and surfaces. The energy with respect to separated CO₂ and metal can, of course, be directly obtained if we subtract the binding energies for CO and oxygen from the CO₂ dissociation energy. Taking Ni as an example it turns out that for a surface the dissociation is exothermic by 0.35 eV [73,74] while it is endothermic for isolated Ni atoms by 0.29 eV [75,76].

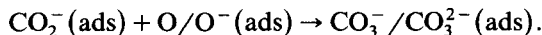
Consulting a recent collection of CO and O binding energies on surfaces published by Toyoshima and Somorjai [77], the values seem to vary greatly depending on the structure of the metal substrate, e.g. surface roughness and crystallinity. For example, the variation in oxygen–metal binding energies is more than five times larger than the difference in exo- and endo-thermicity mentioned above [77]. In other words, for a given metal it will depend on the structure of the surface whether the reaction is thermodynamically allowed [7,8]. Going back to fig. 10, we have shown in the previous paragraphs, that if

we allow the Ni cation to interact with the CO₂ anion a stable Ni–CO₂ cluster is obtained, with a binding energy between 0.39 and 0.58 eV depending on the coordination of CO₂ to the substrate.

For the dissociation of CO₂ into CO and O the mixed carbon–oxygen coordinated configuration ((c) geometry) seems intuitively more likely for several reasons. Firstly, the metal-coordinated C–O bond is elongated with respect to the non-coordinated bond and the electron density on the coordinated oxygen atom has increased, beginning to form the oxygen anion that could bind to the substrate as a surface oxygen (see fig. 2) [29,30]. Also, the CO part begins to assume a geometry similar to the canonical geometry (carbon end down) of CO adsorbed on transition-metal surfaces (see fig. 2) [4]. We can almost imagine what happens: As the coordinated oxygen starts to move away from the carbon it keeps one of the electrons in the C–O single bond while the other bonding electron recouples to the single electron on carbon and forms the CO lone pair that donates into the empty s/p orbitals on the metal [78]. The activation energy for the reverse process, namely CO oxidation, has been shown by Engel and Ertl [3,30] to be 1.07 eV on the Pd(111) surface, which is ≈ 30% of the dissociation energy of CO₂[−] into CO and O[−] as determined above. Considering the pure oxygen coordination, on the other hand, leads us to a different reaction channel.

3.3.2. Oxidation of CO₂

In this section we wish to discuss a reaction path in which the CO₂[−] entity stays intact but binds a surface oxygen to form a carbonate species:



This reaction may occur if CO₂ dissociation is unfavorable. The condition is fulfilled for noble metals. CO₂ dissociation is highly endothermic, e.g. by 2.8 eV for Cu and 3.4 eV for Ag, due to the relatively low binding energies of oxygen (Ag: 1.7 eV [79]; Cu: 2.14 eV [80]) and CO (Ag: 0.28 eV [81]; Cu: 0.62 eV [82]) on these surfaces. However, a prerequisite for such a reaction is the presence of stoichiometric amounts of chemisorbed oxygen on the surface. If we assume this condition to be satisfied, an intuitively appealing starting point for this oxidation reaction is the (b) geometry, see fig. 7b. The unpaired electron on the carbon atom can be used to establish a bond to an unpaired electron of an oxygen atom or an oxygen ion and form, e.g., bidentate or unidentate carbonate. We have calculated the PP orbitals of a carbonate anion and find that the many-electron wavefunction of CO₃^{2−} clearly shows this bond. It is schematically indicated in fig. 7f. We mention in passing that the two Ω bonds formed for CO₂[−] are retained in CO₃^{2−}.

For the stability of CO₃^{2−} with respect to dissociation into CO₂[−] and O[−], resonance is crucial as indicated by the three valence-bond structures in fig. 7f. In fact, it turns out that a single structure is not stable against dissociation by

0.2 eV (table 2). Unfortunately, the full R-GVB calculation is not feasible because of the number of correlated pairs. Therefore, we cannot give a quantitative theoretical estimate for the stability of the carbonate, and there are no experimental data available. For CO₃⁻, however, Castleman and co-workers [83] deduced the experimental dissociation energy of CO₃⁻ into CO₂⁻ and O as 4.33 eV. (For the dissociation into CO₂ and O⁻ a value of 2.27 eV was estimated.) This energy gain is larger than the binding energy of oxygen on a noble-metal surface by ≈ 2 eV. Furthermore, we could expect chemisorbed oxygen to react with CO₂⁻ to form CO₃⁻ on these surfaces. The structure, although not well-known presently, must be considerably different from the one of CO₃²⁻ judged by the vibrational properties [84]. Hartree-Fock calculations by So [85] predict it to have two equivalent short, and one long C-O bonds. This molecule, which is an important intermediate in atmospheric chemistry [86], can possibly pick up an electron and finally form CO₃²⁻, or it actually could be the stable species on the surface.

3.3.3. *Disproportionation of the CO₂ dimer anion*

There is yet another channel through which a surface carbonate can be formed, namely through disproportionation of solvated CO₂⁻:



As we shall see below, there is evidence from reactions of transition-metal compounds for such a mechanism [38,87,88]. We know from our discussion in section 3.2 the structure of the dimer anion (see fig. 8b). If we break a CO bond of CO₂⁻, as alluded to in section 3.3.1, and at the same time form a C-O bond along the arrow in fig. 8b we have disproportionated the dimer anion. The reaction is favored if the binding energy for adsorbed oxygen is smaller than the energy gained by formation of a surface carbonate.

Reactions that can be interpreted as disproportionation reactions of coordinated CO₂ dimers have been reported in organometallic chemistry [38,87,88]. For example, Herskovitz and Guggenberger [87] report the formation of an iridium compound whose structure is shown schematically in fig. 11a. The ligand has been formed by reaction of two CO₂ molecules within the vicinity of the metal. It contains two CO₂ molecules connected by a regular C-O bond. This compound reacts to form products not fully characterized, but assumed to be carbonate and CO-coordinated species. For molybdenum, on the other hand, the corresponding reaction product, a carbonate and a CO-coordinated complex, synthesized via complexation of CO₂, has been characterized by X-ray structure analysis and is shown in fig. 11b [88]. We feel that identification of such compounds [87,88] is a strong indication that disproportionation reactions of this kind may also take place on surfaces. Further evidence is gained from the matrix isolation work of Kafafi et al. [64], who find that the solvated CO₂Li compound mentioned above disproportionates into LiCO₃ and CO.

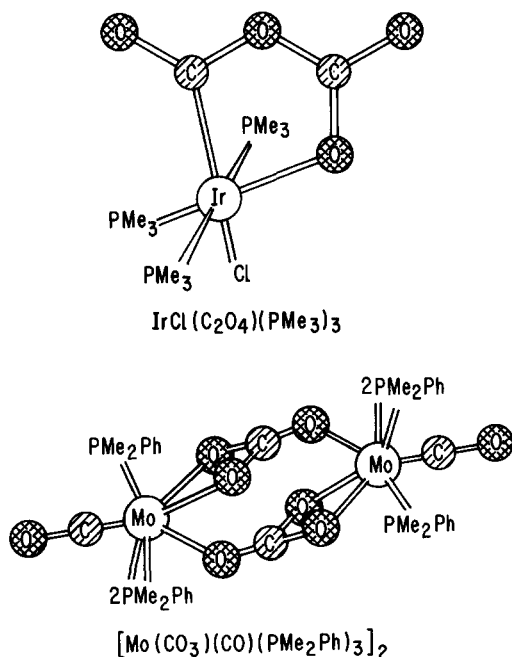


Fig. 11. Schematic structure of a CO₂ dimer complex ($\text{IrCl}(\text{C}_2\text{O}_4)(\text{PMe}_3)_3$) as determined by Herskovitz and Guggenberger [87], and a disproportionated CO₂ dimer complex $[\text{Mo}(\text{CO})_3(\text{CO})(\text{PMe}_2\text{Ph})_3]_2$ as determined by Chatt et al. [88].

3.4. Spectroscopy of CO₂ transition-metal complexes and CO₂ adsorbates

In this section we consider two spectroscopic methods routinely applied to both transition-metal complexes and chemisorbed species, namely vibrational spectroscopy and photoelectron spectroscopy. First we discuss the implications of our findings in the previous sections to photoelectron spectroscopy. As a first crude approximation we use Koopmans' theorem [89] to qualitatively assign the outer valence ionizations. Of course, we are aware of the problems involved in this approximation, and we shall consider the influence of relaxation effects and shake-up excitations in a separate study. Fig. 12 compares graphically the Hartree-Fock one-electron energies of CO₂ and CO₂⁻ with those of O⁻ and CO₃²⁻. CO₂ and CO₂⁻ are reasonably well described at the Hartree-Fock level. If we compare the Koopmans energies of CO₂ with experimental binding energies [90] we find reasonable agreement, the average deviation being 1.9 eV. Since the electron affinity of CO₂ at the Hartree-Fock level is almost the same as at the GVB-PP level (table 2) we assume the Koopmans energies of the anion to represent the photoelectron spectrum of CO₂⁻ with similar accuracy. We have shifted the CO₂⁻ energy scale with respect

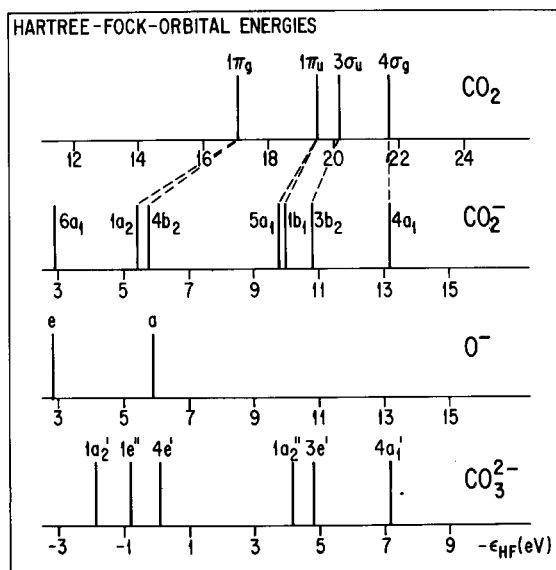


Fig. 12. Hartree-Fock orbital energies of CO₂, CO₂⁻, O⁻, and CO₃²⁻.

to CO₂ so as to line up the lowest-lying outer valence σ orbital. (Note that the shift of ≈ 8.5 eV is equivalent to a Coulomb stabilization if a positive charge were separated by 2.19 Å from the oxygen atoms in C_{2v} symmetry.) For comparison we show in fig. 12 the orbital energies for the oxygen anion on the same energy scale as the CO₂ anion, and the carbonate anion again shifted so as to line up the lowest-lying σ orbital. The broken lines connect corresponding orbitals in CO₂ and CO₂⁻. Four CO₂ ion states (two Π and two Σ states) are predicted and observed in the outer-valence region [90]. One of the Π states (Π_u) originated from the appropriate combination of Ω bonds, the other Π state as well as the two Σ states originate from the four oxygen lone pairs [91]. This is clearly evident from the vibrational structure in the gas-phase photoelectron spectrum [90]. The remaining combination of the four Ω bonds lead to ion states of around 40 eV ionization energy [92]. Upon accommodating the additional electron to form CO₂⁻, the spectrum changes considerably. Firstly, the C_{2v} symmetry of the anion splits all Π levels by a few tenths of an eV. Secondly, the energy separation between some ion states increases considerably. Thirdly, the unpaired electron occupies an orbital (6a₁) unoccupied in the neutral molecule. It appears at lowest binding energy as expected. From the six orbitals originating from the two Π and two Σ states of neutral CO₂ five are now due to oxygen lone pairs. The extra lone pair results from breaking one set of Ω bonds. The 5a₁ orbital represents the new lone pair, while the 1b₁ originates from the remaining set of Ω bonds. The splitting

between the oxygen lone pairs increases with respect to neutral CO₂ due to increasing overlap in the bent geometry. The increase is also consistent with the so-called Walsh rules [93] in molecular-orbital theory. Also, due to the larger electronegativity of oxygen the lone pairs are shifted to lower binding energies on the average. Their position compares well with the outer atomic levels of O⁻ as shown in fig. 12. This shift of the oxygen lone-pair ionizations may be useful analytically in identifying CO₂⁻ on a surface by photoelectron spectroscopy [12]. Unfortunately, a carbonate species, as judged from the Koopmans energies shown in fig. 12, exhibits similar characteristics. Angle-integrated photoelectron spectroscopy as a fingerprint technique may therefore be unable to differentiate the two species. Angle-resolved photoelectron spectroscopy [4], however, could be helpful in distinguishing between CO₂⁻ and CO₃²⁻ because the symmetry of the two anions, and their adsorption geometry are expected to be different.

Let us now very briefly turn to the vibrational properties of CO₂⁻ and carbonate. Table 3 summarizes vibrational frequencies for the most intense vibrational transition in CO₂ and related species, namely the asymmetric stretch. An important observation which can be deduced from table 3 is the strong decrease in the asymmetric stretching frequency from roughly 2350 cm⁻¹ [94] to 1670 cm⁻¹ [44], upon accommodation of an electron. This can be easily explained on the basis of our analysis of the bonding in CO₂⁻. Since the formation of the anion breaks one set of double bonds, the force constant for the C–O bond, after resonating the two valence-bond structures (see fig. 7b), is

Table 3
Asymmetric stretching frequencies of free and coordinated CO₂

System	C–O bond length (Å)	ν (asymmetric stretch) (cm ⁻¹)	Ref.
¹² CO ₂	1.16	2349.16	[94]
¹³ CO ₂	1.16	2283.48	[94]
CO ₂ ⁻	1.22	1671	[44]
LiCO ₂		1570	[64]
LiCO ₂ ·CO ₂		1575	[64]
HCO ₂ H	1.202	1770	[95]
	1.342	1105.3	[95]
(PCy ₃) ₂ Ni(CO ₂)	1.17	1740	[39]
	1.22	1150	[39]
Cp ₂ Mo(CO ₂)	1.20	1745	[96]
	1.29	–	[96]
CO ₃ ²⁻	1.27	1415	[23]
CO ₃ ²⁻ (unidentate)		1480/1370	[23]
CO ₃ ²⁻ (bidentate)		1600/1280	[23]
CO ₃ ²⁻ (organic)		1780/1260	[23]
CO ₃ ⁻		1494/1307	[84]

reduced, leading to a largely reduced stretching frequency. For comparison we show the vibrational frequencies of formic acid [95]. There are two vibrational bands because a C–O double bond (1770 cm^{-1}) can now be differentiated from a single bond (1105 cm^{-1}). Due to mixing of the two vibrational states the given frequencies only approximately represent the isolated bond vibrations. Clearly, the CO₂–metal-coordinated systems show very similar behavior. For the mixed carbon–oxygen-coordinated systems two vibrational frequencies are observed that correspond to the vibration of the long (1150 cm^{-1}) and the short ($1695\text{--}1745\text{ cm}^{-1}$) C–O bond [39,96]. The frequencies are close to the frequencies of formic acid supporting the analogy put forward above. For LiCO₂, for which a structure of C_{2v} symmetry is proposed only one frequency is found [64]. It is $\approx 100\text{ cm}^{-1}$ lower than for free CO₂⁻, namely 1570 cm^{-1} and changes only slightly upon solvation [64]. It should be noted that the formation of a CO₂ anion upon adsorption on surfaces had been proposed very early by Eischens and Pliskin [97] based on the analysis of vibrational spectra.

In summary, we regard the correspondence between CO₂⁻ and Me–CO₂ vibrational frequencies as further evidence for the proposed metal–CO₂ bonding scheme. Using vibrational spectroscopy it should be relatively simple to differentiate between the CO₂⁻ anion and the carbonate as indicated by the collection of carbonate asymmetric-stretching frequencies taken from the literature. In fact, the splitting of the carbonate bands should be a useful criterion to differentiate between various coordination modes, namely flat lying, unidentate, and bidentate (including organic carbonates). It may even be possible to identify the CO₃⁻ anion. Only in organic carbonates are the stretching frequencies at high enough energy to interfere with the CO₂⁻ frequencies.

Acknowledgements

This work was carried out while HJF was a Visiting Research Fellow with the General Electric Research and development Center. He would like to express his sincere gratitude for the financial support as well as for the hospitality accorded to him. We would like to thank Dr. R.C. Tatar and P.A. Schultz for many stimulating discussions on the subject of this paper. H.-J. Freund acknowledges support by the Deutsche Forschungsgemeinschaft and thanks Professor G. Wedler for comments on the manuscript.

References

- [1] E.W. Plummer, in: *Topics in Applied Physics*, Vol. 4, Ed. R. Gomer (Springer, New York, 1975).

- [2] T.N. Rhodin and G. Ertl, Eds., *The Nature of the Surface Chemical Bond* (North-Holland, Amsterdam, 1978).
- [3] T. Engel and G. Ertl, *Advan. Catalysis* 28 (1979) 1.
- [4] E.W. Plummer and W. Eberhardt, *Advan. Chem. Phys.* 49 (1982) 533.
- [5] E.W. Plummer, C.T. Chen, W.K. Ford, W. Eberhardt, R.P. Messmer and H.-J. Freund, *Surface Sci.* 158 (1985) 58.
- [6] (a) D.W. Goodman, D.E. Peebles and J.M. White, *Surface Sci.* 140 (1984) L239, and references therein;
(b) D.E. Peebles, D.W. Goodman and J.M. White, *J. Phys. Chem.* 87 (1983) 4378.
- [7] W.H. Weinberg, *Surface Sci.* 128 (1983) L224, and references therein.
- [8] L.H. Dubois and G.A. Somorjai, *Surface Sci.* 128 (1983) L231, and references therein.
- [9] D.G. Castner and G.A. Somorjai, *Surface Sci.* 83 (1979) 60.
- [10] R.J. Behm and C.R. Brundle, *J. Vacuum Sci. Technol. A1* (1983) 1223.
- [11] W. Spiess, H. Behner, D. Borgmann and G. Wedler, in: *Proc. 3rd Surface Science Symp., Obertraun, Austria, 1985.*
- [12] B. Bartos, H.-J. Freund, H. Kuhlenbeck and M. Neumann, in preparation.
- [13] W. Göpel, R.S. Bauer and G. Hansson, *Surface Sci.* 99 (1980) 138.
- [14] C.T. Campbell and M.T. Paffett, *Surface Sci.* 143 (1984) 517.
- [15] B.A. Sexton and R.J. Madix, *Chem. Phys. Letters* 76 (1981) 294.
- [16] K.C. Prince and A.M. Bradshaw, *Surface Sci.* 126 (1980) 126.
- [17] C. Backx, C.P.M. de Groot, P. Biloen and W.M.H. Sachtler, *Surface Sci.* 128 (1983) 81.
- [18] C.T. Au, S. Singh-Boparai and M.W. Roberts, *J. Chem. Soc. Faraday Trans. I*, 79 (1983) 1779.
- [19] W.H. Cheng and H.H. Kung, *Surface Sci.* 122 (1982) 21.
- [20] M. Bowker, M.A. Barteau and R.J. Madix, *Surface Sci.* 92 (1980) 528.
- [21] M.A. Barteau and R.J. Madix, *Surface Sci.* 97 (1980) 101.
- [22] see e.g. F. Solymosi, A. Erdeöhelyi and T. Bãnsági, *J. Chem. Soc. Faraday Trans. I*, 77 (1981) 2645.
- [23] L.H. Little, *Infrared Spectra of Adsorbed Species* (Academic Press, London, 1966).
- [24] J. Haggin, *Chem. Eng. News*, Feb. 8 (1982) 13.
- [25] (a) R. Bardet, M. Perrin, M. Primet and Y. Trambouze, *J. Chim. Phys.* 75 (1978) 1079;
(b) R. Bardet and Y. Trambouze, *C.R. Hebd. Seances Acad. Sci. Ser. C228* (1979) 101; 290 (1980) 153.
- [26] see e.g. G. Hollemann and K. Wiberg, *Lehrbuch der Anorganischen Chemie* (de Gruyter, Berlin, 1958).
- [27] (a) D.W. Goodman *Acc. Chem. Res.* 17 (1984) 194;
(b) D.W. Goodman, R.D. Kelly, T.E. Madey and J.T. Yates, Jr., *J. Catalysis* 63 (1980) 226.
- [28] H. Körner, H. Landes, G. Wedler and H.J. Kreuzer, *Appl. Surface Sci.* 18 (1984) 361.
- [29] H. Conrad, G. Ertl and J. Küppers, *Surface Sci.* 76 (1978) 232.
- [30] T. Engel and G. Ertl, *J. Chem. Phys.* 69 (1978) 1267.
- [31] R.A. Bair, W.A. Goddard III, A.F. Voter, A.K. Rappe, L.G. Yaffe, F.W. Bobrowicz, W.R. Wadt, P.J. Hay and W.J. Hunt, GVB2P5 program code, unpublished;
R.A. Bair, PhD Thesis, California Institute of Technology (1980);
F.W. Bobrowicz and W.A. Goddard III, in: *Methods of Electronic Structure Theory*, Vol. 3, Ed. H.F. Schaefer III (Plenum, New York, 1977) pp. 79–127;
W.J. Hunt, P.J. Hay and W.A. Goddard III, *J. Chem. Phys.* 57 (1972) 738.
- [32] H.-J. Freund and E.W. Plummer, *Phys. Rev.* B23 (1981) 4859.
- [33] H.-J. Freund, F. Greuter, D. Heskett and E.W. Plummer, *Phys. Rev.* B28 (1983) 1727.
- [34] H.-J. Freund, H. Pulm, B. Dick and R. Lange, *Chem. Phys.* 81 (1983) 99.
- [35] H.-J. Freund, R.P. Messmer, C.M. Kao and E.W. Plummer, *Phys. Rev.* B31 (1985) 4848.
- [36] R. Eisenberg and D.E. Hendricksen, *Advan. Catalysis* 28 (1979) 79.
- [37] D.J. Darenbourg and R.A. Kudoroski, *Advan. Organomet. Chem.* 22 (1983) 129.

- [38] C. Floriani, *Pure Appl. Chem.* 55 (1983) 1.
- [39] (a) M. Aresta, C.F. Nobile, V.G. Albano, E. Forni and M. Manassero, *J. Chem. Soc. Chem. Commun.* (1975) 636;
(b) M. Aresta and C.F. Nobile, *J. Chem. Soc. Dalton Trans.* (1977) 708.
- [40] W. Beck, K. Raab, U. Nagel and M. Steinmann, *Angew. Chem.* 94 (1982) 526.
- [41] S. Sakaki, K. Kiaura and K. Morokuma, *Inorg. Chem.* 21 (1982) 760.
- [42] R.W. Wyckhoff, *Crystal Structures*, 2nd ed., Vol. 1 (Wiley, New York, 1963).
- [43] G. Herzberg, *Electronic Spectra of Polyatomic Molecules* (Van Nostrand, New York, 1966).
- [44] K.O. Hartman and I.C. Hisatsune, *J. Chem. Phys.* 44 (1966) 1913.
- [45] D.W. Ovenall and D.H. Whiffen, *Mol. Phys.* 4 (1961) 135.
- [46] C.D. Cooper and R.N. Compton, *Chem. Phys. Letters* 14 (1972) 29; *J. Chem. Phys.* 59 (1973) 3550.
- [47] C.R. Claydon, G.A. Segal and H.S. Taylor, *J. Chem. Phys.* 52 (1970) 3387.
- [48] J. Pacanski, U. Wahlgren and P.S. Bagus, *J. Chem. Phys.* 62 (1975) 2740.
- [49] W.B. England, *Chem. Phys. Letters* 78 (1981) 607.
- [50] Y. Yoshioka, H.F. Schaefer III and K.D. Jordan, *J. Chem. Phys.* 75 (1981) 1040.
- [51] M.A.F. Gomes and S. Canuto, *J. Phys.* B15 (1982) 1307.
- [52] R.N. Compton, P.W. Reinhardt and C.D. Cooper, *J. Chem. Phys.* 63 (1975) 3821.
- [53] A. Stamatovic, K. Leiter, W. Ritter, K. Stephan and T.D. Märk, *J. Chem. Phys.* 83 (1985) 2942.
- [54] T.D. Märk and A.W. Castleman, Jr., *Advan. At. Mol. Phys.* 20 (1985) 65.
- [55] K.H. Bowen, G.W. Liesegang, R.A. Sanders and D.R. Hershbach, *J. Phys. Chem.* 87 (1983) 557.
- [56] T.H. Dunning, Jr. and P.J. Hay, in: *Methods of Electronic Structure Theory*, Vol. 3, Ed. H.F. Schaefer III (Plenum, New York, 1977) pp. 1–27.
- [57] T.H. Upton and W.A. Goddard III, in: *Chemistry and Physics of Solid Surfaces*, Vol. 3, Eds. T. Vanselow and W.B. England (CRC, Boca Raton, 1982) pp. 127–162.
- [58] The double zeta basis set for the 3d orbital was contracted for the d¹⁰ configuration [taken from an article by A.K. Rappe, T.A. Smedley and W.A. Goddard III, *J. Phys. Chem.* 85 (1981) 2607].
- [59] A.F. Voter and W.A. Goddard III, *Chem. Phys.* 57 (1981) 253.
- [60] L. Pauling, *The Nature of the Chemical Bond* (Cornell Univ. Press, Ithaca, 1960).
- [61] R.P. Messmer, P.A. Schultz, R. Tatar and H.-J. Freund, *Chem. Phys. Letters* 126 (1986) 176.
- [62] C.E. Moore, in: *Atomic Energy Levels*, Vol. II, Natl. Bur. Stand. (US) Spec. Publ. No. 467 (US Govt. Printing Office, Washington, 1952).
- [63] K.D. Jordan, *J. Phys. Chem.* 88 (1984) 2459.
- [64] Z.H. Kafafi, R.H. Hauge, W.E. Billups and J.L. Margrave, *J. Am. Chem. Soc.* 105 (1983) 3886.
- [65] (a) H. Huber, D. McIntosh and G.A. Ozin, *Inorg. Chem.* 16 (1977) 975;
(b) G.A. Ozin, H. Huber and D. McIntosh, *Inorg. Chem.* 17 (1978) 1472.
- [66] A.R. Rossi and K.D. Jordan, *J. Chem. Phys.* 70 (1979) 4422.
- [67] N. Brigot, D. Odiat, S.H. Walmsley and J.L. Whitten, *Chem. Phys. Letters* 49 (1977) 157.
- [68] M.A. Morrison and P.J. Hay, *J. Phys.* B10 (1977) 647.
- [69] A. Terlain and Y. Larcher, *Surface Sci.* 125 (1983) 304.
- [70] J.C. Calabrese, T. Herskovitz and J.B. Kinney, *J. Am. Chem. Soc.* 105 (1983) 5914.
- [71] J. Hölzl and K.F. Schulte, in: *Solid Surface Physics*, Springer Tracts in Modern Physics (Springer, Berlin, 1979).
- [72] H. Hotop and W.C. Lineberger, *J. Phys. Chem. Ref. Data* 4 (1975) 539.
- [73] H.H. Madden, J. Küppers and G. Ertl, *J. Chem. Phys.* 58 (1973) 3401.
- [74] G. Doyen and G. Ertl, *J. Chem. Phys.* 68 (1978) 5417.
- [75] A.E. Stevens, C.S. Feigerle and W.C. Lineberger, *J. Am. Chem. Soc.* 104 (1982) 5026.

- [76] K.P. Huber and G. Herzberg, *Molecular Spectra and Molecular Structure*, Vol. IV. Constants of Diatomic Molecules (Van Nostrand, New York, 1979).
- [77] I. Toyoshima and G.A. Somorjai, *Catalysis Rev. Sci. Eng.* 19 (1979) 105.
- [78] C.M. Kao and R.P. Messmer, *Phys. Rev.* B31 (1985) 4835.
- [79] H.A. Engelhardt and D. Menzel, *Surface Sci.* 57 (1976) 591.
- [80] G. Ertl, *Surface Sci.* 7 (1967) 309.
- [81] G. McElhiney, H. Papp and J. Pritchard, *Surface Sci.* 54 (1976) 617.
- [82] M.A. Chesters, J. Pritchard and M.L. Sims, *Intern. Symp. on Adsorption-Desorption Phenomena*, Florence, 1971.
- [83] D.E. Hunton, M. Hofmann, T.G. Lindeman and A.W. Castleman, Jr., *J. Chem. Phys.* 82 (1985) 134.
- [84] C.W. Chantry, A. Horsefield, J.R. Morton and D.H. Whiffen, *Mol. Phys.* 5 (1962) 589.
- [85] S.P. So, *J. Chem. Soc. Faraday Trans. II*, 72 (1976) 646.
- [86] F. Arnold, in: *Atmospheric Chemistry*, Ed. E.D. Goldberg (Springer, New York, 1982).
- [87] T. Herskovitz and L.J. Guggenberger, *J. Am. Chem. Soc.* 98 (1976) 1615.
- [88] J. Chatt, M. Kubota, G.J. Leigh, F.C. March, R. Mason and D.J. Yarrow, *J. Chem. Soc. Chem. Commun.* (1974) 1033.
- [89] T. Koopmans, *Physica* 1 (1932/33) 104.
- [90] D.W. Turner, A.D. Baker, C. Baker and C.R. Brundle, *Molecular Photoelectron Spectroscopy* (Wiley, New York, 1970).
- [91] P.A. Schultz and R.P. Messmer, to be published.
- [92] H.-J. Freund, H. Kossmann and V. Schmidt, *Chem. Phys. Letters* 123 (1986) 463.
- [93] A.D. Walsh, *J. Chem. Soc.* (1953) 2266.
- [94] G Herzberg, *Infrared and Raman Spectra* (Van Nostrand, New York, 1945).
- [95] T. Shimanouchi, *Tables of Molecular Vibration Frequencies*, NSRDS-Natl. Bur. Stand. Spec. Publ. 39 (1972).
- [96] S. Gambarotta, C. Floriani, A. Chiesi-Villa and C. Guastini, *J. Am. Chem. Soc.* 107 (1985) 2985.
- [97] R.P. Eischens and W.A. Pliskin, *Advan. Catalysis* 9 (1957) 662.